ACS NANO

Cite This: ACS Nano XXXX, XXX, XXX-XXX

www.acsnano.org

ARTICLE

# Pressure-Responsive, Surfactant-Free $CO_2$-Based Nanostructured Fluids

Natascia Grimaldi,[†,‡] Paula Elena Rojas,[†,§] Simon Stehle,[∥,⊥] Alba Cordoba,[‡,§] Ralf Schweins,[▽] Santi Sala,[†,‡,§] Stefan Luelsdorf,[#] David Piña,[†,§] Jaume Veciana,[†,§] Jordi Faraudo,[†] Alessandro Triolo,*[,○] Andreas Siegfried Braeuer,*[,∥,⊥] and Nora Ventosa*[,†,§]

[†]Institut de Ciencia de Materials de Barcelona (ICMAB-CSIC) and [‡]Nanomol Technologies SA, Modul de Recerca B, Campus UAB, 08193 Bellaterra, Spain

[§]Centro de Investigacion Biomedica en Red de Bioingenieria, Biomateriales y Nanomedicina (CIBER-BBN), 28029 Madrid, Spain

[∥]Lehrstuhl für Technische Thermodynamik (LTT), Friedrich-Alexander-Universitaet Erlangen-Nuernberg (FAU), Am Weichselgarten 8, 91058 Erlangen, Germany

[⊥]Erlangen Graduate School in Advanced Optical Technologies (SAOT), Friedrich Alexander-Universitaet Erlangen-Nuernberg (FAU), Paul-Gordan-Straße 6, 91052 Erlangen, Germany

[#]Institut für Physikalische Chemie, Universität Stuttgart, Pfaffenwaldring 55, D-70569 Stuttgart, Germany

[▽]Large Scale Structures Group, Institut Laue-Langevin, 71 Avenue des Martyrs, CS 20156, F-38042 Grenoble Cedex 9, France

[○]Laboratorio Liquidi Ionici, Istituto di Struttura della Materia-CNR (ISM-CNR), Rome 00133, Italy

*Supporting Information*

**ABSTRACT:** **Microemulsions are extensively used in advanced material and chemical processing. However, considerable amounts of surfactant are needed for their formulation, which is a drawback due to both economic and ecological reasons. Here, we describe the nanostructuration of recently discovered surfactant-free, carbon dioxide ($CO_2$)-based microemulsion-like systems in a water/organic-solvent/$CO_2$ pressurized ternary mixture. "Water-rich" nanodomains embedded into a "water-depleted" matrix have been observed and characterized by the combination of Raman spectroscopy, molecular dynamics simulations, and small-angle neutron scattering. These single-phase fluids show a reversible, pressure-responsive nanostructuration; the "water-rich" nanodomains at a given pressure can be instantaneously degraded/expanded by increasing/decreasing the pressure, resulting in a reversible, rapid, and homogeneous mixing/demixing of their content. This pressure-triggered responsiveness, together with other inherent features of these fluids, such as the absence of any contaminant in the ternary mixture (*e.g.*, surfactant), their spontaneous formation, and their solvation capability (enabling the dissolution of both hydrophobic and hydrophilic molecules), make them appealing complex fluid systems to be used in molecular material processing and in chemical engineering.**

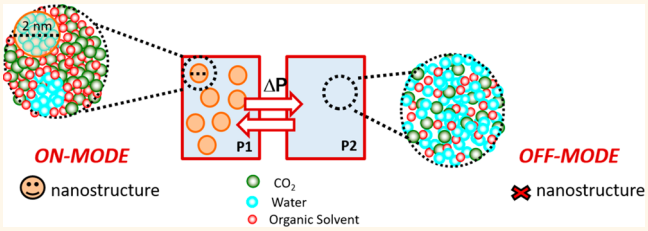


**KEYWORDS:** *surfactant-free, compressed $CO_2$, microemulsion, nanostructured fluids, Raman, SANS, MD simulations, neutron scattering*

Microemulsions are macroscopically homogeneous, isotropic, and thermodynamically stable systems, containing at least three compounds: a polar one, usually water, a nonpolar one, usually oil, and an amphiphilic compound, usually a surfactant.[1] These macroscopically homogeneous systems are nanostructured in "oil-rich" and "water-rich" domains, which can show various size and shape, depending on the composition and the environmental conditions.[2] The structuration at the nanoscale entails other specific properties of microemulsions, such as ultralow interfacial tension,[3,4] large interfacial area,[5] and the ability to solubilize otherwise immiscible compounds.[1,2] As they contain both a polar and a nonpolar solvent, microemulsions have been considered as universal solvents. Accordingly, they are very appealing systems either as commercial products or as reaction media for many processes, ranging from nanoparticle templates to preparative confined organic chemistry.[1,6] Furthermore, as they form spontaneously, their preparation process is considered facile and of low cost. However, a significant

Received: April 11, 2017
Accepted: August 28, 2017
Published: August 28, 2017





DOI: 10.1021/acsnano.7b02500
ACS Nano XXXX, XXX, XXX−XXX

disadvantage of conventional microemulsions is their reliance on the use of—sometimes highly concentrated and environmentally malign—surfactants, which are required in order to thermodynamically stabilize the system. This in turn, affects their sustainability both in terms of costs and environmental impact.

$CO_2$-based microemulsions and surfactant-less or surfactant-free microemulsions have been extensively investigated as valuable greener alternatives to conventional microemulsions since the late 1970s, but only recently their structure has been investigated at the mesoscopic scale.[7−11] In $CO_2$-based microemulsions, the oil phase is substituted by compressed $CO_2$ ($cCO_2$). Compared to organic solvents, $cCO_2$ is low cost, nonflammable, environmentally benign, bio- and food-compatible, and naturally abundant. Generally, $CO_2$ is a poor solvent, in particular for polar and/or high molecular weight solutes,[13] but when dissolved in water in the presence of specific surfactants, a water/$CO_2$-based microemulsion is formed. Mainly, fluorinated or partly fluorinated surfactants have been used in order to form $CO_2$-based microemulsions. However, they are expensive and environmentally unviable, and nowadays many efforts are made in the design of small-cheap-safe molecules able to stabilize the water/$CO_2$ interface.[13−18] Water/$CO_2$-based microemulsions have the attractive characteristics of $cCO_2$ and the solvation properties of bulk water, being a universal solvent for many applications. Furthermore, because of the presence of $cCO_2$, the properties of these unconventional microemulsions, such as density, and hence solvation power, can be strongly modified just by pressure variation.[11,12] The latter feature is very attractive both from the fundamental and technical point of view. This pressure responsiveness of the emulsion's properties is significantly less pronounced in conventional microemulsions,[19] where in order to change the microemulsion's properties, composition and/or temperature are the more appropriate tuning parameters.

In this context, we recently reported on the structuration of the single-phase mixture water/acetone/$CO_2$ into "water-rich" and "water-depleted" regions at 10 MPa and 308 K. It has to be underlined that the structuration was observed in the single-phase region, far from the critical point of the ternary mixture.[20] Moreover, it has been already reported that this pressurized mixture shows the capability to solubilize non-water and non-$CO_2$ soluble compounds, which are soluble in acetone and in $CO_2$-expanded acetone, such as ibuprofen. Indeed, the addition of $CO_2$ over an equimolar water/acetone mixture saturated with ibuprofen, where a solid phase and a liquid phase coexist at 10 MPa and 308 K, induces the solubilization of the precipitated $CO_2$-phobic drug. This behavior can be explained if the addition of $CO_2$ causes a structuration at the nanoscale in "water-rich" regions and in "water-depleted" domains, where the ibuprofen is dissolved (see SI for more details).[20,21]

The here studied structured single-phase system is referred to as "microemulsion-like system" rather than microemulsion,[20] as it is not clear yet whether or not the acetone takes over the role of the surfactant. In this paper, we report on the nanostructuration of differently composed water/acetone/$CO_2$ mixtures, at various temperatures (298, 308, and 328 K) and pressures (10, 14, 18, and 22 MPa), by means of Raman spectroscopy. Moreover, we also describe the nanostructuration of pressurized mixtures of water/acetonitrile/$CO_2$. Molecular dynamics (MD) simulations were performed to study the molecular nanostructuration with atomistic detail. The size of the "water-rich" domains in these pressurized mixtures was experimentally characterized by high-pressure small-angle neutron scattering (hp-SANS). By using hp-SANS we have also observed that the nanostructure is pressure responsive, in a reversible way. These single-phase, nanostructured fluids have several of the favorable properties of conventional microemulsions in terms of interfacial properties, solvent capability, and ability to act as templates (nanocontainers), with the advantages of being "green" and showing a reversible, pressure-responsive nanostructure. We expect that by pressure changes, we can instantaneously tune the extent of the fluid's nanostructure, resulting in a rapid and homogeneous exchange of species between the multiple nanodomains, that is, mixing/demixing of the fluid. This can open not yet anticipated pathways in process engineering, making these nanostructured pressure-responsive fluids appealing systems to be used in molecular material processing and in chemical engineering.

## RESULTS/DISCUSSION

The tendency of water molecules to aggregate in the different pressurized ternary mixtures of water/acetone/$CO_2$ and water/acetonitrile/$CO_2$ and to form a thermodynamically stable single-phase fluid with "water-rich" nanodomains embedded into a "water-depleted" matrix has been explored, using a range of complementary experimental and computational techniques.

Figure 1 shows schematic Gibbs phase diagrams of the different ternary systems water/organic-solvent/$CO_2$ at 10 MPa studied.

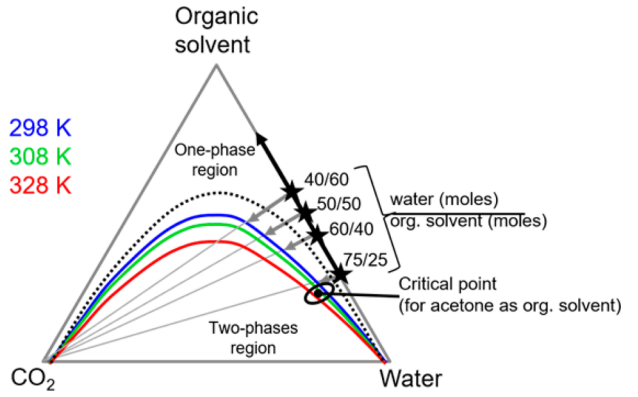


**Figure 1. Schematic Gibbs diagrams of the ternary systems water/organic-solvent/$CO_2$ based on data from literature (refs 22 and 23) and data reported in Table 1. Solid colored lines show qualitatively the binodals of the system water/acetone/$CO_2$ (10 MPa) at 298 K (blue), 308 K (green), and 328 K (red). For the system water/acetonitrile/$CO_2$, the binodal has been measured experimentally at 308 K and 10 MPa and is shown by the dotted line (see SI). The gray arrows show the $CO_2$ dilution paths of the initial "water/acetone" systems when $CO_2$ is added to the mixture until the binodal. The solid black arrow shows the organic solvent dilution path when the initial mixtures are diluted by the addition of more organic solvent.**

The colored solid curves were extracted from refs 22 and 23 and were partly measured (see Table 1), showing qualitatively the binodals of the system water/acetone/$CO_2$ at three different temperatures, which separate the single-phase region from the two-phase region. The dotted curve corresponds to the binodal of the system water/acetonitrile/$CO_2$ at 308 K and 10 MPa, and it has been experimentally determined (see SI).



DOI: 10.1021/acsnano.7b02500
ACS Nano XXXX, XXX, XXX−XXX

**Table 1. $CO_2$ Molar Fraction $x_{CO_2}$ (± 0.001) at the Binodal of the Ternary Mixture Water/Acetone/$CO_2$[a]**

| | | $x_{CO_2}$ | | |
|---|---|---|---|---|
| $P$ (MPa) | initial water/acetone molar ratio | 298 K | 308 K | 328 K |
| 10 | 50/50 | 0.158 | 0.170 | 0.192 |
| | 60/40 | 0.115 | 0.121 | 0.126 |
| | 75/25 | 0.051 | 0.056 | 0.061 |
| 14 | 50/50 | – | 0.182 | – |
| 18 | 50/50 | – | 0.190 | – |
| 22 | 50/50 | – | 0.198 | – |

[a]When water/acetone mixtures of different initial molar ratios (50/50, 60/40, and 75/25) are diluted with $CO_2$ either at 10 MPa but at different temperatures or at 308 K but at different pressures.

The solid black arrow on the water/organic solvent (acetone or acetonitrile) axis shows the dilution path when an initial binary water/organic-solvent mixture (marked with a star) is diluted with additional acetone (or acetonitrile). The gray arrows show for 298 K the $CO_2$ dilution paths when an initial binary water/acetone mixture is diluted with $CO_2$ in the single-phase region (not exceeding the binodal). Depending on the nature of the organic solvent (acetone vs acetonitrile) as well as on the starting binary mixture composition or the temperature or pressure, the length of the $CO_2$ dilution path in the single-phase region (before intersection with the binodal) varies.

Table 1 lists the experimentally determined locations where the $CO_2$-dilution path (gray arrows in Figure 1), starting with different initial water/acetone mixture compositions, crosses the binodal, for the ternary mixture water/acetone/$CO_2$ at various pressures and temperatures. With increasing temperature, the molar fraction of $CO_2$ at the crossing point of the binodal and the $CO_2$-dilution-path increases, while the fractions of acetone and water slightly decrease. All dilution paths were realized isothermally and isobarically in a variable-volume high-pressure chamber. With dilution, the total amount of water molecules in the variable-volume high-pressure chamber is constant, while the water concentration in "moles per liters" decreases when the volume of the chamber has to be varied in order to dilute isobarically.

Intuitively, if the water concentration decreases homogeneously, less hydrogen bonds between water molecules are formed. For example, the number of hydrogen bonds decreases monotonically, if an initial binary water/acetone mixture is diluted with additional acetone at 10 MPa and 308 K (black arrow mixing path in Figure 1), as it has been demonstrated in Hankel *et al.*[20] and as it is shown in the Supporting Information (SI). On the contrary, if the dilution induces a nanostructuration into "water-concentrated" regions, containing many water molecules, and "water-less-concentrated" regions, containing few water molecules, the number of hydrogen bonds increases. Experimentally, this can be studied by the use of Raman spectroscopy; while diluting, we analyzed the frequency (energy) of the symmetric water stretch vibration band. From the shape of this Raman band, the development of hydrogen bonds can be extracted. In particular, we use the Raman shift $\overline{\nu}_{water}$ in wavenumbers ($cm^{-1}$) of the centroid of the symmetric water stretch vibration Raman broad band for the characterization of the development of hydrogen bonds, as described in the SI. The smaller $\overline{\nu}_{water}$ is, the more hydrogen bonds are developed in the mixture.[24−27]

**The Ternary System Water/Acetone/$CO_2$.** Figure 2 shows the Raman shift of the centroid of the symmetric water stretch vibration band $\overline{\nu}_{water}$ as a function of the water concentration $c_{water}$ for the dilution of three different binary

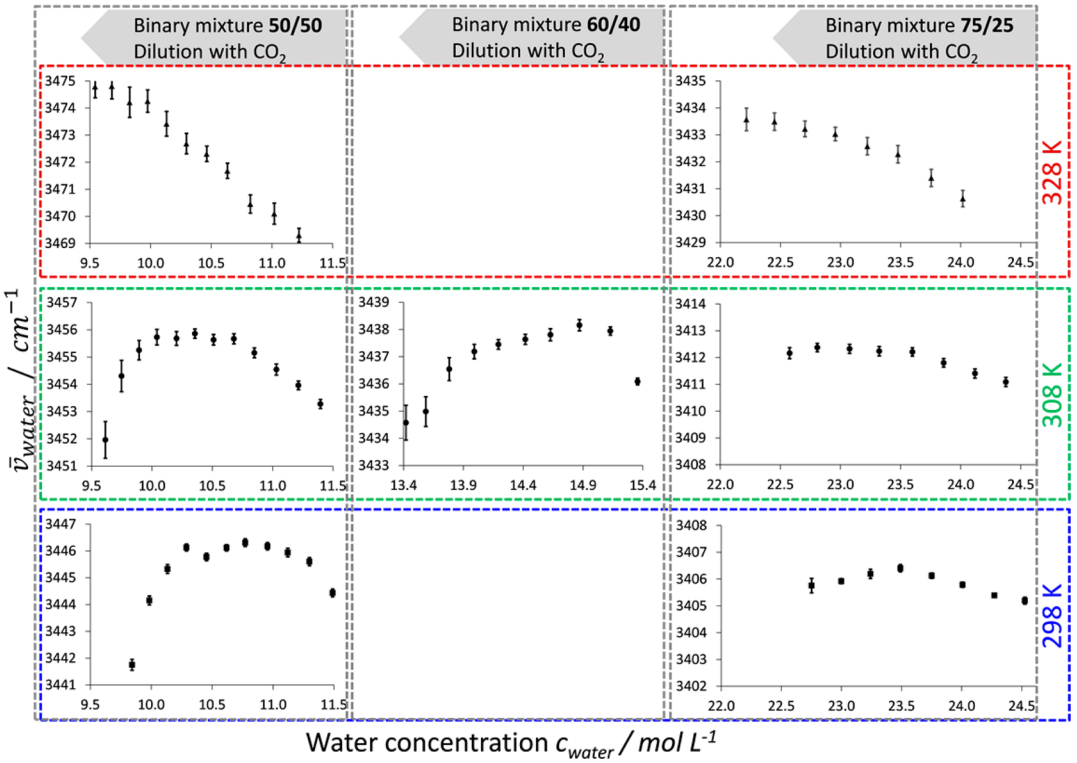


**Figure 2. $\overline{\nu}_{water}$ as a function of the water concentration $c_{water}$ when three initially binary water/acetone mixtures are diluted with $CO_2$ at 298, 308, and 328 K at 10 MPa. Only one temperature (308 K) was analyzed for the initial 60/40 water/acetone binary mixture.**



DOI: 10.1021/acsnano.7b02500
ACS Nano XXXX, XXX, XXX−XXX

mixtures of water/acetone (molar ratio) 50/50, 60/40, and 75/25 (columns in Figure 2) upon the addition of $CO_2$ at 298, 308, and 328 K (lines in Figure 2) at a pressure of 10 MPa. In each subfigure of Figure 2, the dilution of the initially binary water/acetone mixtures (right data points) with $CO_2$ goes from large to small water concentration values (from right to left). The left data points are the last measurements made in the single-phase region. A further dilution with $CO_2$ drove the mixture across the binodal into the two-phase region. Thus, all the data points shown in the figure correspond to mixture compositions in the single-phase region of the ternary system, before crossing the binodal. Each data point is the average of 200 single Raman measurements. The acquisition of one Raman spectrum took 5 s. The standard deviation of $\bar{\nu}_{water}$ is given by the error bars. While the ordinate of each subfigure covers consistently a range of six wavenumbers, the absolute values of $\bar{\nu}_{water}$ vary significantly from subfigure to subfigure. The smallest values of $\bar{\nu}_{water}$ can be found at 298 K for the $CO_2$ dilution of the initial 75/25 water/acetone mixture, which implies that at the lower temperatures and the larger water concentrations, many hydrogen bonds are developed. The largest values of $\bar{\nu}_{water}$ can be found at 328 K for the $CO_2$ dilution of the initial 50/50 water/acetone mixture, which implies that at the higher temperatures and the smaller water concentrations, less hydrogen bonds are developed.

The data measured for 328 K show the behavior expected for a system that does not develop a nanostructuration. The Raman shift of the centroid of the symmetric water stretch vibration band $\bar{\nu}_{water}$ increases monotonically with decreasing $c_{water}$, irrespectively of the composition of the initial water/acetone mixture. Therefore, at 328 K the development of hydrogen bonds gets less pronounced with increasing $CO_2$ dilution. For 308 K and 298 K, the data rows show a maximum of $\bar{\nu}_{water}$. Starting from the initial binary mixtures, $\bar{\nu}_{water}$ first increases with $CO_2$ dilution, until the maximum of $\bar{\nu}_{water}$ is reached, and then decreases with further $CO_2$ dilution.

Therefore, at 308 K and 298 K, the development of hydrogen bonds with increasing $CO_2$ dilution first declines to a minimum, which is the maximum of $\bar{\nu}_{water}$, and then rises. The rise of the development of hydrogen bonds with increasing $CO_2$ dilution is due to the emergence of a nanostructuration of the ternary mixture in "water-concentrated" regions containing many water molecules and "water-depleted" regions containing few water molecules. This hypothesis will be further underlined by small-angle neutron scattering (SANS) experiments and by MD simulations. The overall change of $\bar{\nu}_{water}$ during one $CO_2$ dilution experiment increases with increasing temperature from 298 K to 308 K and with decreasing water content in the initial binary water/acetone mixture. For the $CO_2$ dilution of the 75/25 initial binary water/acetone-mixture at 308 K, a maximum of $\bar{\nu}_{water}$ is hardly detectable. Finally we want to underline that the $CO_2$ dilution path starting from the initial 75/25 binary water/acetone mixture is the closest to the critical point of the ternary system. For this $CO_2$ dilution path, we find the smallest change of $\bar{\nu}_{water}$ as a function of the water concentration. Therefore, we can conclude that the nanostructuration we observed is different from critical fluctuations, which would reach their maximum at the mixture critical point.[26]

Figure 3 shows the Raman shift of the centroid of the symmetric water stretch vibration band $\bar{\nu}_{water}$ as a function of the $CO_2$ molar fraction $x_{CO_2}$ for the dilution of initial 50/50

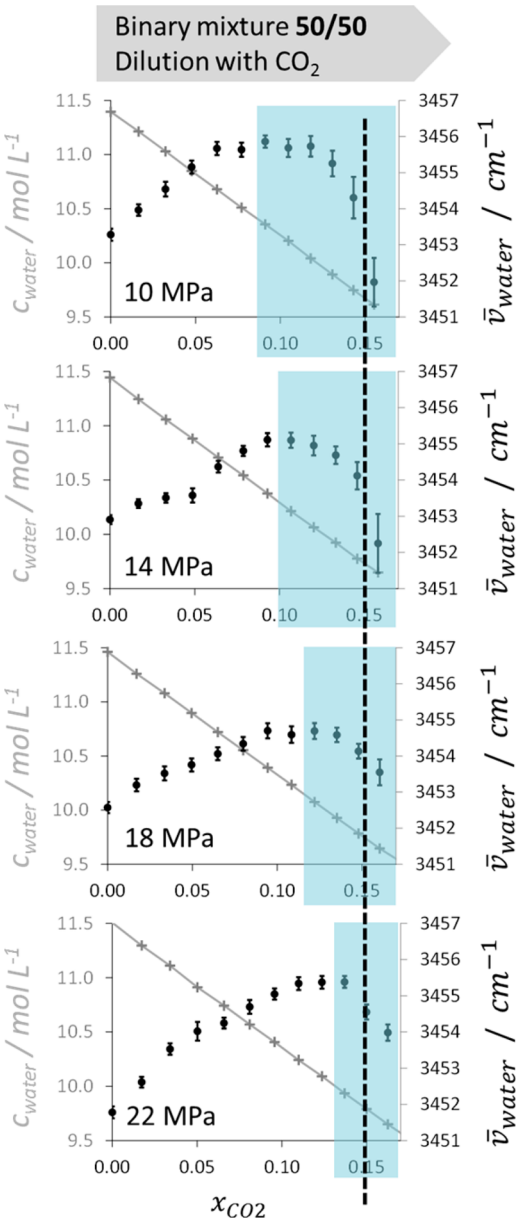


**Figure 3. $\bar{\nu}_{water}$ (right ordinate) as a function of the $CO_2$ molar fraction $x_{CO_2}$ of the ternary mixture water/acetone/$CO_2$ when binary water/acetone mixtures of an initial 50/50 molar relation are diluted with $CO_2$ at 308 K and at 10, 14, 18, and 22 MPa. The water concentration as a function of the $CO_2$ molar fraction is also given (left ordinate). Regions of nanostructuration are highlighted in blue.**

water/acetone mixtures at 308 K for pressures of 10, 14, 18, and 22 MPa. In contrast to Figure 2, in Figure 3 we scale on the abscissa the $CO_2$ molar fraction $x_{CO_2}$ instead of the water concentration, $c_{water}$. This assures a better comparability with the hp-SANS results that follow. Nevertheless, the $CO_2$ molar fractions $x_{CO_2}$ are correlated with the corresponding water concentrations $c_{water}$ on the left ordinate. As the dilution is realized by the addition of $CO_2$, the $CO_2$ dilution in Figure 3 proceeds from left to right, meaning that the very left data points correspond to the binary water/acetone mixtures at 308 K at the different pressures before the addition of $CO_2$. The very right data points represent the last measurement made in



DOI: 10.1021/acsnano.7b02500
ACS Nano XXXX, XXX, XXX−XXX

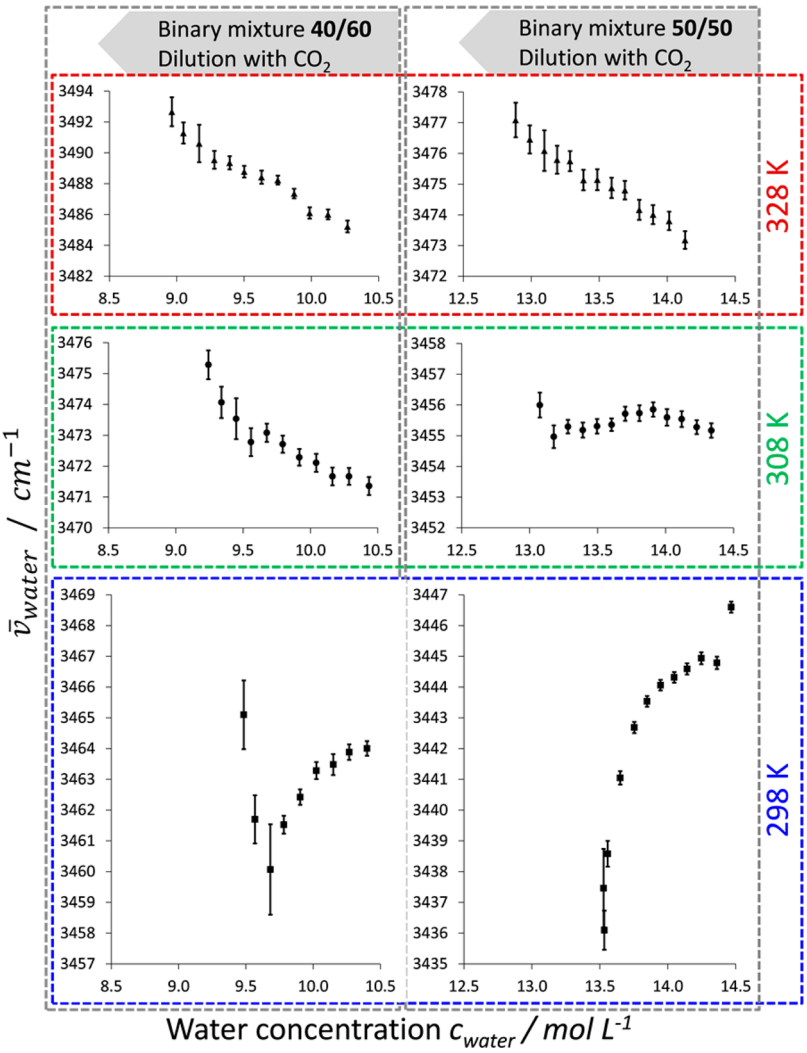


**Figure 4. $\bar{\nu}_{water}$ as a function of the water concentration $c_{water}$ when two initially binary water/acetonitrile mixtures with 40/60 and 50/50 molar relationships are diluted with $CO_2$ at 298, 308, and 323 K, at 10 MPa.**

the single-phase region. A further addition of $CO_2$ drove the system across the binodal into the two-phase region. As already mentioned above, the experimentally determined compositions of the binodal are shown in Table 1.

In each subfigure in Figure 3 the ordinate quantifying $\bar{\nu}_{water}$ comprises six wavenumbers (cm$^{-1}$). Irrespective of pressure (within the analyzed range), $\bar{\nu}_{water}$ first increases when the system is diluted by the addition of $CO_2$ (from left to right). Therefore, the development of hydrogen bonds first decreases until the maximum of $\bar{\nu}_{water}$ is reached. With further addition of $CO_2$ the system undergoes a nanostructuration in "water-concentrated" regions containing many water molecules and "water-depleted" regions containing few water molecules, which is expressed by the decrease of $\bar{\nu}_{water}$. The higher the pressure is, the larger $CO_2$ molar fractions are required for the initialization of the nanostructuration (this is highlighted in Figure 3 by blue shadows). A ternary mixture with a $CO_2$ molar fraction of $x_{CO_2}$ = 0.15 at 10 MPa and 308 K (upper subfigure) is further in the region of nanostructuration than a mixture with the same composition but at higher pressure and the same temperature (lower subfigures). With increasing pressure, the minimum $x_{CO_2}$ value, for which nanostructuration is detectable (maximum of $\bar{\nu}_{water}$), moves to larger $x_{CO_2}$ values and at the same time also the $x_{CO_2}$ values that correspond to the binodal increase (see Table 1).

**The Ternary System Water/Acetonitrile/$CO_2$.** Figure 4 shows the Raman shift of the centroid of the symmetric water stretch vibration band $\bar{\nu}_{water}$ as a function of the water concentration for the dilution of two different binary mixtures of water/acetonitrile with 50/50 and 40/60 molar relationships. At 328 K $\bar{\nu}_{water}$ increases monotonically with $CO_2$ dilution, irrespective of the initial mixture composition. This indicates that with $CO_2$ dilution, the hydrogen bonds develop less. At 298 K, $\bar{\nu}_{water}$ decreases from the very beginning of the $CO_2$ dilution, irrespective of the initial binary mixture composition indicating that initially more hydrogen bonds develop. The maximum development of hydrogen bonds is found for 298 K at the minimum of $\bar{\nu}_{water}$.

For the ternary systems water/acetone/$CO_2$ and water/acetonitrile/$CO_2$ at 10 MPa, we can summarize that the behavior of $\bar{\nu}_{water}$ as a function of the water concentration $c_{water}$ significantly depends on the temperature. At the highest analyzed temperature of 328 K, $\bar{\nu}_{water}$ increased monotonically with $CO_2$ dilution for each initial binary mixture composition. Whereas at the lowest analyzed temperature of 298 K, $\bar{\nu}_{water}$ decreased with $CO_2$ dilution either from the very beginning or


DOI: 10.1021/acsnano.7b02500
ACS Nano XXXX, XXX, XXX−XXX

after reaching a maximum. At the intermediate temperature of 308 K, the behavior of $\overline{\nu}_{water}$ as a function of $c_{water}$ is in between the behaviors identified for 298 and 328 K. With this observation together with the temperature sensitivity of the binodal curves shown in Figure 1 and Table 1, we can deduce that, for a given initial binary mixture composition, the behavior of $\overline{\nu}_{water}$ as a function of $c_{water}$ depends on the length of the $CO_2$ dilution path in the single-phase region, before phase separation, or in other words on the solubility (quantified as $CO_2$ molar fraction) of $CO_2$ in the ternary mixture. This statement is also underlined by the results shown in the context of the pressure variation (Figure 3). Again we can deduct from Table 1 that for the 50/50 initial binary water/acetone mixture, the behavior of $\overline{\nu}_{water}$ as a function of $x_{CO_2}$ depends on the length of the $CO_2$ dilution path in the single-phase region, before phase separation, or in other words on the solubility (quantified as $CO_2$ molar fraction) of $CO_2$ in the ternary mixture at various pressures. The lower the solubility of $CO_2$ in the ternary water/organic solvent/$CO_2$ mixtures is, the more pronounced is the extent of nanostructuration in "water-concentrated" regions and "water-depleted" regions (see Table 1).

**Dimensions and Shape of "Water-Rich" Nanodomains.** SANS succeeds in probing structural heterogeneities over spatial scales on the order of several Å up to 100 nm and, as such, has been successfully exploited by several teams to characterize microemulsion systems over mesoscopic spatial scales.[2,27] Here, in order to get direct structural insight into the complex mesoscopic organization of the pressurized water/organic solvent/$CO_2$ systems, we used a specially designed high-pressure SANS cell.[28]

In Figure 5, the hp-SANS data are presented for different mixtures water/deuterated acetone/$CO_2$ at 308 K and 10 MPa, as a function of the dissolved amount of $CO_2$ and as a function of the water concentration $c_{water}$. These data sets are plotted together with the pattern of the binary equimolar mixture water/deuterated acetone at the same experimental conditions (pressure, temperature). While the latter data set shows a small excess scattering with respect to the flat incoherent scattering due to hydrogen, in agreement with previous determinations,[29,30] upon $CO_2$ addition a distinct increase of the scattering amplitude can be observed in the low $Q$ range that is presently accessed ($0.01 \leq Q$ (Å) $\leq 0.1$). This fingerprints the progressive development of structural heterogeneities with spatial extent of the order of a few nanometers. Related scattering studies that were focused on other surfactant-free microemulsion systems (*e.g.*, water/ethanol/octanol)[7−10,31] highlighted comparable diffraction features in the low $Q$ portion of the SANS patterns. The present hp-SANS data sets have been modeled in terms of the Ornstein−Zernike (O-Z) model that allows to estimate the characteristic size of the structural heterogeneities responsible for the excess low $Q$ scattering, namely:

$$I(Q) = I(0)/(1 + Q^2\xi^2) + \text{bkg}$$

where $I(0)$ represents the normalized scattering intensity at zero angle and $\xi$ is the spatial extent of the structural heterogeneities.[7]

In the inset of Figure 5, the $CO_2$ content dependence of $\xi$ is shown, indicating that when adding $CO_2$ to the water/acetone equimolar mixture, the formation of segregated clusters (nanostructuration) occurs, whose spatial extent grows with $CO_2$ content and reaches a size of approximately 2.5 nm at $x_{CO_2}$ = 0.14 ($c_{water}$ = 9.682 mol $L^{-1}$). This finding correlates well with the decrease of the centroid of the Raman band $\overline{\nu}_{water}$ with $CO_2$ dilution for water concentrations between 10.5 and 9.5 mol $L^{-1}$ for the ternary system water/acetone/$CO_2$ at 308 K and 10 MPa reported in Figure 2.

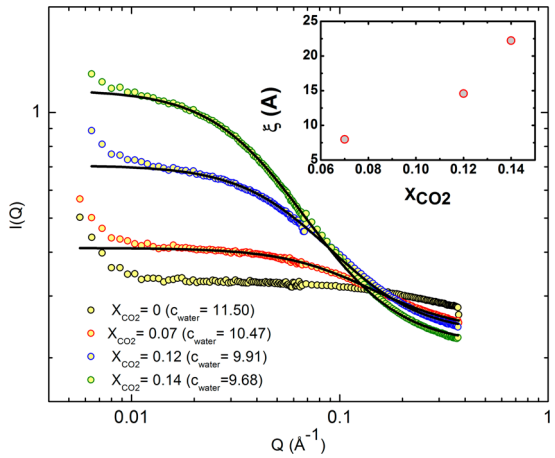


**Figure 5. SANS curves of water/deuterated acetone/$CO_2$ mixtures, with $x_{water} = x_{acetone} = (1 - x_{CO_2})/2$ and $x_{CO_2}$ = 0, 0.07, 0.12, and 0.14 ($c_{water}$ = 11.50, 10.47, 9.91, 9.68 mol $L^{-1}$) at 308 K and 10 MPa. The lines refer to fits of experimental data to the Ornstein−Zernike model, excluding the $Q$ portion below 0.01 Å. The upturn might reflect larger structural heterogeneities that the present hp-SANS experiment does not provide access to. In the inset, the dependence of the characteristic size for the structural heterogeneities as a function of the $CO_2$ molar fraction responsible for the low $Q$ excess scattering is plotted.**

**Molecular Dynamics Simulations.** Using MD simulations, we can provide an atomistic interpretation of the experimental results. To this end, we performed all-atomic MD simulations of water/acetone and water/acetone/$CO_2$ mixtures with eight different water concentrations at 10 MPa and 308 K (see Methods for technical details). In each MD simulation we started with binary mixtures of water and acetone ($x_{water}$ = $x_{acetone}$ = 0.5). For the dilution with acetone we added more acetone molecules to the initial mixture, obtaining binary mixtures with decreasing molar fractions of water (black arrow in Figure 1). For the $CO_2$ dilution path, we added more $CO_2$ molecules (gray arrow in Figure 1). In this way we obtained simulations of ternary water/acetone/$CO_2$ mixtures with different amounts of $CO_2$, keeping constant the number of acetone and water molecules. Note that all simulations contain the same number of water molecules. In the first set of simulations, the water concentration decreases due to the addition of acetone, while in the second simulation set, the water concentration decreases due to the addition of $CO_2$.

For all simulations we computed the number $N_{w-w}$ of hydrogen bonds of each water molecule with other water molecules (water−water hydrogen bonds), and we divided this quantity by the result obtained for the initial water/acetone 50/50 mixture, $N_{w-w}^{(0)}$. The resulting ratio, $R_{Hbonds} = N_{w-w}/N_{w-w}^{(0)}$ is shown in Figure 6. As it can be seen in Figure 6, the dilution with acetone induces a decrease of $R_{Hbonds}$ as the concentration of water decreases. On the contrary, in the case of dilution with $CO_2$, we observe a nearly constant $R_{Hbonds}$, though the concentration of water decreases. In fact, a careful


DOI: 10.1021/acsnano.7b02500
ACS Nano XXXX, XXX, XXX−XXX

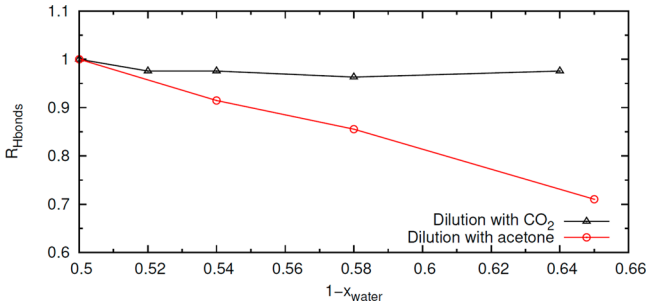


**Figure 6. Evolution of the number of water−water hydrogen bonds in MD simulations at 308 K and 10 MPa after dilution of an initial water/acetone 50/50 mixture. We consider dilution by adding acetone (circles) or $CO_2$ (triangles). $R_{Hbonds}$ is defined as the ratio between the number of water−water hydrogen bonds observed in a particular simulation divided by the number of water−water hydrogen bonds obtained in the initial water/acetone 50/50 mixture which contains the same number of water molecules.**

look at Figure 6 shows a very weak dependence of $R_{Hbonds}$ with water concentration in the ternary system, with a slight decrease of $R_{Hbonds}$ to a minimum and a subsequent slight increase. The simulation results reported in Figure 6 are in complete agreement with the interpretation of Raman experiments provided in the previous section and in our previous work.[20]

The nanostructuration postulated by the analysis of Raman and SANS experimental results can also be seen in our MD simulations. In Figure 7, we show simulation images for a ternary mixture with $x_{CO_2}$ = 0.15 and $x_{water}$ = $x_{acetone}$ = 0.425. As it can be seen in Figure 7a, acetone molecules are homogeneously distributed over the whole system, but water is localized in pockets containing hydrogen-bonded water molecules. These water pockets induce inhomogeneities in the water density profiles (see Figure S7 in the SI), which have a typical length scale of ∼2 nm. Inside these water pockets, water molecules form hydrogen-bonded chain structures, as illustrated in Figure 7b (see also the pair correlation functions reported in Figure S8 in the SI). The average number of hydrogen bonded neighbors of a water molecule is 2. On average, we found that in these chain-like structures, 48% of the water molecules have two hydrogen bonds, and with other water molecules, 28% had only one and 24% more than 2 hydrogen bonds. Acetone also makes hydrogen bonds with water through the carbonyl group (Figure 7b), as demonstrated by the sharp peak in the acetone−water pair correlation function (Figure S8 in the SI). $CO_2$ molecules avoid contact with water-concentrated pockets. The broad peaks in the $CO_2$ correlation functions (Figure S8 in the SI indicates that $CO_2$ molecules tend to be coordinated both with other $CO_2$ molecules and acetone molecules). In Figure 7c we also show a typical configuration contributing to these broad peaks in the $CO_2$−$CO_2$ and $CO_2$−acetone correlation functions. Typically, we found two or three $CO_2$ molecules (with C−C distance about 4 Å) surrounded by acetone molecules (with a peak at a carbon−carbon separation of 4.4 Å). Water also tends to be anticorrelated with (effectively repelled by) $CO_2$, up to distances of about 1 nm.

**Pressure-Responsiveness of Nanostructured, Single-Phase Liquid.** The hp-SANS measurements were performed at different pressures. For this study the ternary mixture water/deuterated acetone/$CO_2$ with $x_{CO_2}$ = 0.15 ($x_{water}$ = $x_{acetone}$ =

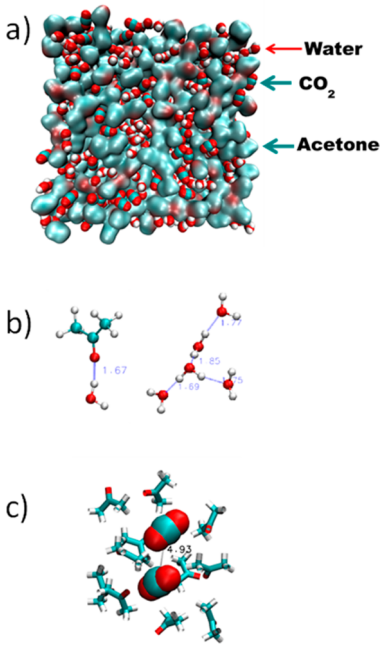


**Figure 7. Images from MD simulations of the water/acetone/$CO_2$ ternary mixture (10 MPa and 308 K, $x_{CO_2}$ = 0.15, $x_{water}$ = 0.425). (a) Simulation snapshot. Water and $CO_2$ molecules are shown as spheres with van der Waals radius. Acetone molecules (which form a network across the system) are shown as a surface calculated using the molecular surface solver of VMD28 with a 1.4 Å probe radius. The employed color code is red for O, white for H, and cyan for C. (b) A water-acetone hydrogen bond and a water hydrogen-bonded chain configuration extracted from (a) (all molecules are shown in CPK representation). (c) Detail of a pair of $CO_2$ molecules (in van der Waals representation) surrounded by acetone molecules (shown in bonds representation) in a configuration extracted from (a). Hydrogen-bond distances are given in angstroms.**

0.425) at 10 MPa and 308 K was used. The effect of the increase of pressure, from 10 to 30 MPa, was determined by a stepwise pressure increase in increments of 4 MPa. After that, the pressure is reduced back from 30 to 10 MPa, in order to rule-out any hysteresis phenomenon. The data are presented in Figure 8 as a function of pressure. In particular, the description of the scattering data in terms of the O-Z model allows detecting a progressive decrease of the scattering amplitude upon pressure increase. The isothermal compressibility of the ternary water/acetone/$CO_2$ mixture ($x_{water}$ = $x_{acetone}$ = 0.43 and $x_{CO_2}$ = 0.14) as a function of pressure was measured and is shown in Figure S2a in the SI, aiming at addressing the source of scattering amplitude decrease. The ternary mixture has a lower isothermal compressibility than that of pure $CO_2$[32] (4.1 × $10^{-2}$ to 5.5 × $10^{-3}$ $MPa^{-1}$ for pure $CO_2$ and 6.8 × $10^{-4}$ to 6.9 × $10^{-4}$ $MPa^{-1}$ for the ternary mixture, respectively). In fact, the values of compressibility we measured for the ternary mixture at elevated pressure are between the corresponding compressibility values of pure water and pure acetone at ambient conditions. Moreover, the compressibility of the ternary mixture slightly increases with pressure (<2%), showing an opposite trend to that observed for pure $CO_2$ (pronounced decrease, *ca.* 80%, Figure S2b in the SI). According to the relationship $I(0)= nK_BT\kappa$[33] (where $n$ is the number density of scatterers (heterogeneities), $K_B$ is Boltzmann constant, $T$ is temperature, and $\kappa$ is the isothermal compressibility), the low $Q$


DOI: 10.1021/acsnano.7b02500
ACS Nano XXXX, XXX, XXX−XXX

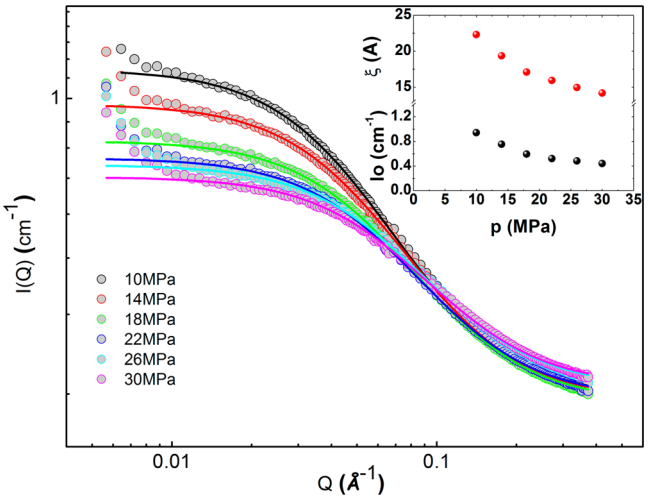


**Figure 8. SANS curves for the system water/deuterated acetone/$CO_2$, with $x_{water}$ = $x_{acetone}$ = 0.425 and $x_{CO_2}$ = 0.15 at 308 K and different values of pressure in the range between 10 and 30 MPa. The lines refer to fits of experimental data to the Ornstein−Zernike model, excluding the Q range below 0.01 Å$^{-1}$. In the inset, the pressure dependence of scattering amplitude and characteristic size for the structural heterogeneities are shown.**

limit of the normalized scattering intensity $I(0)$ should increase with increasing pressure, following the trend of the compressibility of the ternary mixture. In Figure 8, the opposite trend is observed. We can then rule out the effect of compressibility in affecting the amplitude of the low Q scattering and directly relate it to the decreasing average size of the segregated domains with increasing pressure (see inset of Figure 8), which is proportional to the scattering domains' volume. All of these observations reveal that these single-phase fluids feature a pressure-responsive extent of nanostructuration. This finding allows proposing pressure as an effective tool to affect the segregated morphology in these systems. Similar conclusions were drawn from the results shown in Figure 3, where we saw that the higher the pressure is, the more $CO_2$ is needed for the appearance of the nanostructuraction. This, in other words, means that at equal composition (*i.e.*, $x_{water}$ = $x_{acetone}$ = 0.425 and $x_{CO_2}$ = 0.15) and temperature, the extent of the nanostructuraction is tunable by pressure.

Furthermore, hp-SANS was used to monitor the reversibility of the formation of the nanostructuration upon cyclic pressure jumps. In Figure 9, we show two different data sets at 14 and 30 MPa that were obtained by raising the pressure (14 → 30 MPa in several steps), then decreasing (30 → 14 MPa in several steps) it, and then raising (14 → 30 MPa in one step) it again. As it can be seen, the two data sets obtained at the same nominal pressure nicely lay on top of each other, thus providing experimental support to the reversibility of the extent of nanostructuration upon pressure modulation.

## CONCLUSIONS AND FUTURE PERSPECTIVES

The combination of Raman spectroscopy, hp-SANS, and MD simulations provides valuable complementary insights into the appearance of "water-rich" nanodomains within the pressurized, single-phase mixtures of water/organic solvent/$CO_2$, both in the case of acetone and acetonitrile being the organic solvent.

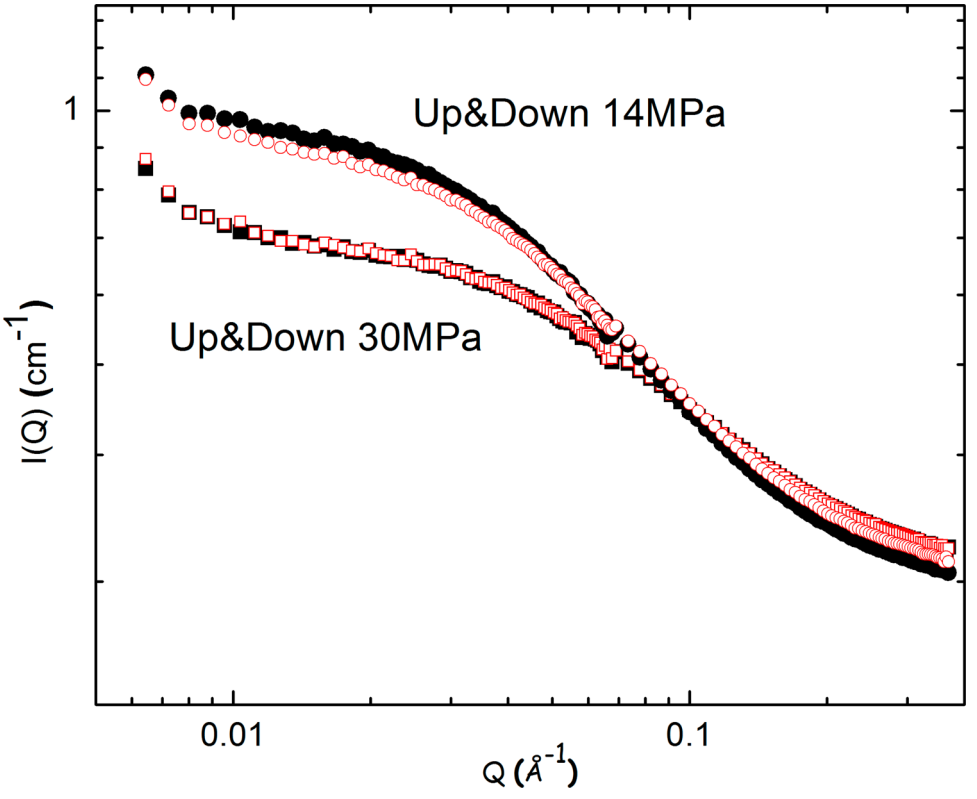


**Figure 9. SANS curves for system water/deuterated acetone/$CO_2$, with $x_{water}$ = $x_{acetone}$ = 0.425 and $x_{CO_2}$ = 0.15 at 308 K and 14 or 30 MPa. The different data sets at a given pressure refer to different routes used to reach these pressure values, aiming at confirming the lack of process hysteresis in the formation/decomposition of nanoaggregates.**



DOI: 10.1021/acsnano.7b02500
*ACS Nano* XXXX, XXX, XXX−XXX

Raman spectroscopy reveals the occurrence of water molecules aggregation, that is, the formation of "water-concentrated" regions, and clarifies how the thermodynamic conditions, that is, composition, temperature, and pressure, affect this phenomenon. hp-SANS measurements provide information about the characteristic size of these "water-rich" nanodomains, and MD simulations clarify how the molecules are localized within the ternary mixture and supports experimental findings. The final outcome is that these ternary mixtures water/organic solvent/$CO_2$ can turn into a surfactant-free microemulsion-like system, where "water-concentrated" nanodomains, with a characteristic size of the order of 2 nm, are embedded in a "water-depleted" matrix. The aggregation of water molecules occurs when $CO_2$ is added to a binary mixture of water/organic solvent. hp-SANS measurements show that the nanostructure of these surfactant-free fluids can be reversibly tuned by pressure variations. We can distinguish between an "ON" state, where the nanostructuraction is occurring at a large extent, and an "OFF" state, where by progressively increasing the pressure (above 10 MPa), the medium remains macroscopically homogeneous, but the structural heterogeneities start to drastically decrease in their extent (see the abstract graphic). This reversible, pressure responsiveness is completely missed in conventional microemulsions, where changes in their nanoscopic structure require temperature and/or compositional variations, which propagate much slower through the mixture, thus making jumps in the activating parameters (temperature or concentration) less efficient and/or less homogeneous. We expect to exploit the herein presented pressure responsiveness together with the already proved solvent capability of these nanostructured green fluids[20] (see Figure S9 in the SI for more details) in order to use them in chemical and process engineering. In fact, if we think to apply the revealed "water-rich" nanodomains embedded in a water-depleted matrix as nanocontainers, when in "ON" mode, then these nanocontainers can instantaneously be destroyed by pressure changes, resulting in a rapid and homogeneous mixing/demixing of the containers' contents. From the technological point of view, by using these fluids we can imagine to create innovative pathways in process engineering and for the manufacturing of products with a high degree of control over material properties.

## METHODS

**Microemulsion Preparation and Materials.** Nanostructured systems have been prepared in a homemade, high-pressure visual variable volume cell (HPVVVC), which is described in the SI (Figure S1). Acetone (Uvasol) and acetonitrile (LiChrosolv) purchased from Merck Millipore (Germany) both with a purity of 99.9% as well as $CO_2$ 4.5 purchased from Linde (Germany) with a purity of 99.995% were used without further purification. Water was highly purified (conductivity <18 $\mu$S cm$^{-1}$) in house by an ion-exchange water system (SG 2800 SK, SG Wasseraufbereitung and Regenerierstation, Germany). For hp-SANS measurements, acetone (Uvasol) has been replaced by its perdeuterated form (99.9 atom % D) purchased from Sigma-Aldrich and used without further purification.

**Experimental Characterization.** The miscibility gap of the ternary mixture was identified using the cloud-point method as described in detail in the SI. Data have been collected for water/organic solvent/$CO_2$ mixtures at various compositions and temperatures. The Raman spectra of water, acetone, $CO_2$, and their mixtures have been acquired using the setup described in the SI (Figure S3) and are reported in Figure S4. The water symmetric stretch vibration band has been isolated from the Raman spectrum of the mixture as described in SI. The Raman shift (wavenumber position) of the centroid of the isolated symmetric water stretch vibration signal was computed and considered as an indicator for the development of hydrogen bonds. Small Raman shift values of the centroid indicate that many hydrogen bonds are developed. Large Raman shift values of the centroid indicate that few hydrogen bonds are developed. High-pressure small-angle neutron scattering (hp-SANS) measurements were performed at the Institut Laue-Langevin (Grenoble, FR) (beamline D11). Data were collected using an incident neutron wavelength of 6 Å with 9% fwhm and working at two different sample−detector distances (1.75 and 10 m); this setup allows reaching a momentum transfer range between 0.007 and 3.5 Å$^{-1}$. A high-pressure cell, previously described by Pütz *et al.*, was utilized for the measurements.[34,35] Further technical details are provided in the SI.

**Computer Simulations.** The all atomic molecular dynamics (MD) simulations reported here were performed using the NAMD 2.9 software[36] with a thermostat at 308 K and a barostat at 10 MPa. In our simulations, water was described employing the TIP4P/2005 model,[37] which is known to correctly reproduce the phase diagram of water, both at low and high pressures.[38] This model is also the best available in reproducing the hydrogen-bonding features of liquid water at all pressures.[39] $CO_2$ and acetone were described using the CGenFF version of the CHARMM force field.[40] We performed four simulations of a binary water/acetone mixture and also four simulations of the ternary water/acetone/$CO_2$ mixture, all corresponding to different compositions but always at 308 K and 10 MPa. The first simulation was performed with a binary mixture with initially the same number of acetone and water molecules ($x_{water} = x_{acetone}$). This simulation was the starting point for two different simulations series, one series corresponding to dilution with acetone (binary water/acetone mixtures) and the second series corresponding to dilution with $CO_2$ (water/acetone/$CO_2$ ternary mixtures). Note that the ternary water/acetone/$CO_2$ mixture simulations correspond to different amounts of $CO_2$ but always with $x_{water} = x_{acetone}$. Further details of the simulation protocol are described in the SI.

## ASSOCIATED CONTENT

### Supporting Information

The Supporting Information is available free of charge on the ACS Publications website at DOI: 10.1021/acsnano.7b02500.

Further information regarding experimental determination of the ternary Gibbs diagrams, isothermal compressibility, the development of hydrogen bonds, and the correlation lengths of the structural heterogeneities using hp-SANS. Qualitative description of the solubilization of ibuprofen in nanostructured water/acetone/$CO_2$ mixtures. Additional information on MD simulations (PDF)

## AUTHOR INFORMATION


### Corresponding Authors

*E-mail: triolo@ism.cnr.it.
*E-mail: andreas.braeuer@fau.de.
*E-mail: ventosa@icmab.es.

### ORCID

Jaume Veciana: 0000-0003-1023-9923
Alessandro Triolo: 0000-0003-4074-0743
Nora Ventosa: 0000-0002-8008-4974


### Notes

The authors declare no competing financial interest.

## ACKNOWLEDGMENTS

N.G. acknowledges the European Commission (EC) (FP7-PEOPLE-2013-Initial Training Networks (ITN) "'NANO2-FUN'" project no. 607721) for her Postdoctoral contract. A.S.B. thanks funding from the European Research Council



DOI: 10.1021/acsnano.7b02500
ACS Nano XXXX, XXX, XXX−XXX

under ERC starting grant agreement no. 637654. The authors appreciate the economical support from DGI, MINECO, Spain (Grant MAT2016-80826-R and "Severo Ochoa" Programme for Centres of Excellence in R&D (SEV- 2015-0496)), and the Instituto de Salud Carlos III, through "Acciones CIBER". The ICTS "Nanbiosis", more specifically U6 Unit, is also acknowledged since some of the studies here reported have been performed there. Neutron beam time at the Institut Laue-Langevin (ILL) Grenoble, France, is acknowledged together with Dr. Thomas Sottmann, who has kindly provided the high-pressure cell used for SANS measurements. The authors acknowledge the valuable support of Julian Jonathan Schuster from FAU with respect to the processing of Raman spectra and the valuable help of David Bowyer during experiments at ILL.

## REFERENCES

(1) *Microemulsions: Backgrounds, New Concepts, Applications, Perspectives*; Stubenrauch, C., Ed.; John Wiley & Sons, Ltd: Chichester, UK, 2009.
(2) Strey, R. Microemulsion Microstructure and Interfacial Curvature. *Colloid Polym. Sci.* **1994**, *272* (8), 1005−1019.
(3) Fletcher, D. I.; Horsup, D. I. Droplet Dynamics in Water-in-Oil Microemulsions and Macroemulsions Stabilised by Non-Ionic Surfactants. Correlation of Measured Rates with Monolayer Bending Elasticity. *J. Chem. Soc., Faraday Trans.* **1992**, *88*, 855−864.
(4) Sottmann, T.; Strey, R. Ultralow Interfacial Tensions in Water-*n*-Alkane-Surfactant Systems. *J. Chem. Phys.* **1997**, *106*, 8606−8615.
(5) Sottmann, T.; Strey, R.; Chen, S. H. A Small-Angle Neutron Scattering Study of Nonionic Surfactant Molecules at the Water-Oil Interface: Area per Molecule, Microemulsion Domain Size, and Rigidity. *J. Chem. Phys.* **1997**, *106*, 6483−6491.
(6) López Quintela, M. L.; Tojo, C.; Blanco, M.; Rio, L. G.; Leis, J. Microemulsion Dynamics and Reactions in Microemulsions. *Curr. Opin. Colloid Interface Sci.* **2004**, *9*, 264−278.
(7) Diat, O.; Klossek, M. L.; Touraud, D.; Deme, B.; Grillo, I.; Kunz, W.; Zemb, T. Octanol-Rich and Water-Rich Domains in Dynamic Equilibrium in the Pre-Ouzo Region of Ternary Systems Containing a Hydrotrope. *J. Appl. Crystallogr.* **2013**, *46*, 1665−1669.
(8) Schöttl, S.; Touraud, D.; Kunz, W.; Zemb, T.; Horinek, D. Consistent Definitions of "The Interface" in Surfactant-Free Micellar Aggregates. *Colloids Surf., A* **2015**, *480*, 222−227.
(9) Prevost, S.; Lopian, T.; Pleines, M.; Diat, O.; Zemb, T. Small-Angle Scattering and Morphologies of Ultra-Flexible Microemulsions. *J. Appl. Crystallogr.* **2016**, *49*, 2063−2072.
(10) Zemb, T. N.; Klossek, M.; Lopian, T.; Marcus, J.; Schöettl, S.; Horinek, D.; Prevost, S. F.; Touraud, D.; Diat, O.; Marčelja, S.; Kunz, W. How to Explain Microemulsions Formed by Solvent Mixtures without Conventional Surfactants. *Proc. Natl. Acad. Sci. U. S. A.* **2016**, *113*, 4260−4265.
(11) Eastoe, J.; Yan, C.; Mohamed, A. Microemulsions with $CO_2$ As a Solvent. *Curr. Opin. Colloid Interface Sci.* **2012**, *17*, 266−273.
(12) Triolo, F.; Triolo, A.; Triolo, R.; Londono, J. D.; Wignall, G. D.; McClain, J. B.; Betts, D. E.; Wells, S.; Samulski, E. T.; DeSimone, J. M. Critical Micelle Density for the Self-Assembly of Block Copolymer Surfactants in Supercritical Carbon Dioxide. *Langmuir* **2000**, *16*, 416−421.
(13) Klostermann, M.; Foster, T.; Schweins, R.; Lindner, P.; Glatter, O.; Strey, R.; Sottmann, T. Microstructure of Supercritical $CO_2$-in-Water Microemulsions: A Systematic Contrast Variation Study. *Phys. Chem. Chem. Phys.* **2011**, *13*, 20289−20301.
(14) Yan, C.; Sagisaka, M.; James, C.; Rogers, S. E.; Peach, J.; Hopkins Hatzopoulos, M.; Eastoe, J. Action of Hydrotropes in Water-in-$CO_2$ Microemulsions. *Colloids Surf., A* **2015**, *476*, 76−82.
(15) Klostermann, M.; Strey, R.; Sottmann, T.; Schweins, R.; Lindner, P.; Holderer, O.; Monkenbusch, M.; Richter, D. Structure and Dynamics of Balanced Supercritical $CO_2$- Microemulsions. *Soft Matter* **2012**, *8*, 797−807.
(16) Clarke, M. J.; Harrison, K. L.; Johnston, K. P.; Howdle, S. M. Water in Supercritical Carbon Dioxide Microemulsions: Spectroscopic Investigation of a New Environment for Aqueous Inorganic Chemistry. *J. Am. Chem. Soc.* **1997**, *119*, 6399−6406.
(17) Ray, S.; Moulik, S. Phase Behavior, Transport Properties, and Thermodynamics of Water/AOT/Alkanol Microemulsion Systems. *J. Colloid Interface Sci.* **1995**, *173*, 28−33.
(18) Peach, J.; Eastoe, J. Supercritical Carbon Dioxide: A Solvent Like no Other. *Beilstein J. Org. Chem.* **2014**, *10*, 1878−1895.
(19) Rudolph, E. S. J.; Bovendeert, M. J.; De Loos, Th.W.; De Swaan Arons, J. Influence of Methane on the Phase Behavior of Oil + Water + Nonionic Surfactant Systems. *J. Phys. Chem. B* **1998**, *102*, 200−205.
(20) Hankel, R. F.; Rojas, P. E.; Cano-Sarabia, M.; Sala, S.; Veciana, J.; Braeuer, A.; Ventosa, N. Surfactant-Free $CO_2$-Based Microemulsion-Like Systems. *Chem. Commun.* **2014**, *50* (60), 8215−8218.
(21) Muntó, M.; Ventosa, N.; Sala, S.; Veciana, J. Solubility Behavior of Ibuprofen and Naproxen Drugs in Liquid "$CO_2$-Organic Solvent" Mixture. *J. Supercrit. Fluids* **2008**, *47*, 147−153.
(22) Wendland, M.; Hasse, H.; Maurer, G. Multiphase High-Pressure Equilibria of Carbon Dioxide-Water-Acetone. *J. Supercrit. Fluids* **1994**, *7* (4), 245−250.
(23) Lazzaroni, M. J.; Bush, D.; Jones, R.; Hallett, J. P.; Liotta, C. L.; Eckert, C. A. High-Pressure Phase Equilibria of some Carbon Dioxide−Organic−Water Systems. *Fluid Phase Equilib.* **2004**, *224* (1), 143−154.
(24) Barlow, S. J.; Bondarenko, G. V.; Gorbaty, Y. E.; Yamaguchi, T.; Poliakoff, M. An IR Study of Hydrogen Bonding in Liquid and Supercritical Alcohols. *J. Phys. Chem. A* **2002**, *106*, 10452−10460.
(25) Carey, D. M.; Korenowski, G. M. Measurement of the Raman Spectrum of Liquid Water. *J. Chem. Phys.* **1998**, *108*, 2669−2675.
(26) Kazarian, S. G.; Gupta, R. B.; Clarke, M. J.; Johnston, K. P.; Poliakoff, M. How is Hydrogen-Bonding Influenced by Solvent Density? The Spectroscopic Study and Modeling of the Interaction between a Proton Donor and Acceptor from the Gas Phase to Supercritical Fluid States. *J. Am. Chem. Soc.* **1993**, *115*, 11099−11109.
(27) Nave, S.; Eastoe, J.; Heenan, R. K.; Steytler, D.; Grillo, I. What is So Special About Aerosol-OT? 2. Microemulsion Systems. *Langmuir* **2000**, *16* (23), 8741−8748.
(28) Pütz, Y. $CO_2$ Microemulsions with Additives: Phase Behavior, Microstructure and Pressure-Induced Kinetics. Ph.D. Thesis, University of Cologne: Cologne, Germany, 2015.
(29) McLain, S. E.; Soper, A. K.; Luzar, A. Investigations on the Structure of Dimethyl Sulfoxide and Acetone in Aqueous Solution. *J. Chem. Phys.* **2007**, *127*, 174515.
(30) Perera, A.; Sokolić, F.; Almásy, L.; Westh, P.; Koga, Y. On the Evaluation of the Kirkwood-Buff Integrals of Aqueous Acetone Mixtures. *J. Chem. Phys.* **2005**, *123*, 024503.
(31) Schöttl, S.; Marcus, J.; Diat, O.; Touraud, D.; Kunz, W.; Zemb, T.; Horinek, D. Emergence of Surfactant-Free Micelles from Ternary Solutions. *Chem. Sci.* **2014**, *5*, 2949.
(32) Span, R.; Wagner, W. A. New Equation of State for Carbon Dioxide Covering the Fluid Region from the Triple-Point Temperature to 1100 K at Pressures up to 800 MPa. *J. Phys. Chem. Ref. Data* **1996**, *25* (6), 1509−1596.
(33) Kotlarchyk, M.; Chen, S. H.; Huang, J. S.; Kim, M. W. Structure of Three Component Microemulsions in the Critical Region Determined by Small-Angle Neutron Scattering. *Phys. Rev. A: At., Mol., Opt. Phys.* **1984**, *29*, 2054−2069.
(34) Klossek, M. L.; Touraud, D.; Zemb, T.; Kunz, W. Structure and Solubility in Surfactant-Free Microemulsions. *ChemPhysChem* **2012**, *13*, 4116−4119.
(35) Müller, A.; Pütz, Y.; Oberhoffer, R.; Becker, N.; Strey, R.; Wiedenmann, A.; Sottmann, T. Kinetics of Pressure Induced Structural Changes in Super- or Near-Critical $CO_2$ -Microemulsions. *Phys. Chem. Chem. Phys.* **2014**, *16*, 18092.
(36) Phillips, J. C.; Braun, R.; Wang, W.; Gumbart, J.; Tajkhorshid, E.; Villa, E.; Chipot, C.; Skeel, R. D.; Kale, L.; Schulten, K. Scalable Molecular Dynamics with NAMD. *J. Comput. Chem.* **2005**, *26*, 1781−1802.


DOI: 10.1021/acsnano.7b02500
*ACS Nano* XXXX, XXX, XXX−XXX

(37) Abascal, J. L. F.; Vega, C. A General Purpose Model for the Condensed Phases of Water: TIP4P/2005. *J. Chem. Phys.* **2005**, *123* (23), 234505.
(38) Vega, C.; Abascal, J. L. F. Simulating Water with Rigid Non-Polarizable Models: A General Perspective. *Phys. Chem. Chem. Phys.* **2011**, *13* (44), 19663−19688.
(39) Calero, C.; Martí, J.; Guàrdia, E. $^{1}$H Nuclear Spin Relaxation of Liquid Water from Molecular Dynamics Simulations. *J. Phys. Chem. B* **2015**, *119* (5), 1966−1973.
(40) Vanommeslaeghe, E.; Hatcher, C.; Acharya, S.; Kundu, S.; Zhong, J.; Shim, E.; Darian, O.; Guvench, P.; Lopes, I.; Vorobyov, A. D.; MacKerell, Jr. CHARMM General Force Field (Cgenff): A Force Field for Drug-Like Molecules Compatible with the CHARMM All-Atom Additive Biological Force Fields. *J. Comput. Chem.* **2010**, *31*, 671−690.



DOI: 10.1021/acsnano.7b02500
*ACS Nano* XXXX, XXX, XXX−XXX